Perovskites

How to cite:
International Edition: doi.org/10.1002/anie.202007520
German Edition: doi.org/10.1002/ange.202007520

Stereoselective C–C Oxidative Coupling Reactions Photocatalyzed by Zwitterionic Ligand Capped $CsPbBr_3$ Perovskite Quantum Dots

*Yucheng Yuan, Hua Zhu, Katie Hills-Kimball, Tong Cai, Wenwu Shi, Zichao Wei, Hanjun Yang, Yolanda Candler, Ping Wang, Jie He, and Ou Chen**

Abstract: *Semiconductor quantum dots (QDs) have attracted tremendous attention in the field of photocatalysis, owing to their superior optoelectronic properties for photocatalytic reactions, including high absorption coefficients and long photogenerated carrier lifetimes. Herein, by choosing 2-(3,4-dimethoxyphenyl)-3-oxobutanenitrile as a model substrate, we demonstrate that the stereoselective (>99%) C–C oxidative coupling reaction can be realized with a high product yield (99%) using zwitterionic ligand capped $CsPbBr_3$ perovskite QDs under visible light illumination. The reaction can be generalized to different starting materials with various substituents on the phenyl ring and varied functional moieties, producing stereoselective dl-isomers. A radical mediated reaction pathway has been proposed. Our study provides a new way of stereoselective C–C oxidative coupling via a photocatalytic means using specially designed perovskite QDs.*

Introduction

Semiconductor quantum dot (QD) nanocrystals (NCs) have been exploited in diverse practical applications including solar energy harvesting,[1] biological imaging and labeling,[2] light-emitting diodes,[3] and next-generation displays,[4] owing to their superior optical and optoelectronic properties.[5] Recently, QDs have shown great promise as efficient photocatalysts for organic reactions such as oxidation,[6] reduction,[7] and redox reactions,[8] taking advantages of their high photo- and chemical stabilities,[5b,c] large absorption coefficients,[9] high quantum efficiencies,[10] as well as long photo-generated carrier lifetimes.[11] Additionally, comparing to metal complexes or organic dyes, colloidal QDs as photocatalysts exhibit several unique advantages. Firstly, colloidal QDs can act as both photosensitizers and catalysts simultaneously, surpassing conventional photocatalytic systems where photosensitizers and catalysts are usually distinct species.[12] Secondly, unlike conventional Ru or Ir complex-based catalysts, typical QDs (CdS, CdSe, InP QDs, or perovskite QDs) do not contain precious metals. Thirdly, surface ligands of the QDs can be engineered without altering the redox potentials or the absorption profiles of the QDs, in contrast to coordination compounds whose electronic structure can be greatly altered by ligand identities. Finally, the band gaps of QDs, thus the redox potentials, can be customized for different catalytic reactions through tuning the size, shape and/or composition of the QDs. To date, conventional metal chalcogenide (for example, CdSe and CdS) QDs have been heavily investigated and demonstrated as efficient photocatalysts for a series of organic reactions including C–C couplings,[6b,c,8a,b,13] dehalogenations,[13a,14] oxidations,[6c,13a,15] polymerizations,[16] and cyclizations.[8d,17] In contrast, perovskite QDs, owing to their young age and commonly reported stability issues, have been less explored in photocatalytic organic reactions.[18] Successful examples include degradations of organic dyes,[19] thiol coupling,[20] C–H activation,[8e,20] and polymerizations.[6a] Furthermore, it was rarely reported that QDs photocatalyzed bond formations could proceed with control of stereoselectivity. To the best of our knowledge, the only example is the CdSe QDs photocatalyzed diastereoselective intermolecular [2+2] cycloadditions, which were achieved by the self-assembly of the substrate molecules on the QD surface.[8d] Besides, perovskite QDs photocatalyzed reactions with stereoselectivity have not yet been realized until now. Given the superior photochemical and optoelectronic properties of perovskite QDs, their full potentials in the utilization as unique and efficient photocatalysts still need to be further explored while resolving the drawback of their instability issues.

Herein, we demonstrate that $CsPbBr_3$ perovskite QDs can successfully photocatalyze the stereoselective C–C oxidative homocoupling of α-aryl ketonitriles under visible light illumination. Through the surface modification of $CsPbBr_3$ perovskite QDs with zwitterionic ligands, the NC stability and homocoupling reaction rate can be dramatically increased, and the stereoselectivity can be significantly improved. A reaction scope study shows that electron-donating groups (EDGs) or large conjugated π systems are necessary for the efficient dimerization. We propose that the reaction undergoes a radical intermediate reaction pathway on the surface of the perovskite QDs, in which a less steric hinderance leads to the favored *dl*-isomer. The produced dimers, which are hardly

[*] Dr. Y. Yuan, Dr. H. Zhu, Dr. K. Hills-Kimball, T. Cai, W. Shi, H. Yang, Y. Candler, Prof. P. Wang, Prof. O. Chen
Department of Chemistry, Brown University
324 Brook St., Providence, RI 02912 (USA)
E-mail: ouchen@brown.edu
Z. Wei, Prof. J. He
Department of Chemistry, University of Connecticut
55 North Eagleville Rd., Storrs, CT 06269 (USA)
Prof. P. Wang
State Key Laboratory of Electroanalytical Chemistry, Changchun Institute of Applied Chemistry, Chinese Academy of Sciences
Changchun 130022, Jilin (P.R.China)
Supporting information and the ORCID identification number(s) for the author(s) of this article can be found under: https://doi.org/10.1002/anie.202007520.

accessible using other oxidants or catalysts,[21] can be used as intermediates to form indenes with significant pharmaceutical potentials.[22] Our study suggests that colloidal perovskite QDs with proper surface modifications are promising photocatalysts in chemical transformations and organic syntheses.

Results and Discussion

To explore and compare different QDs as photocatalysts for the C–C oxidative coupling of α-aryl ketonitriles, we synthesized eight types of QDs with different compositions and capping ligands (Table 1; Supporting Information, Figures S1–S3). In particular, zwitterionic ligand (that is, 3-(*N*,*N*-dimethyloctadecylammonio)propanesulfonate, DMOA-PS) capped colloidal $CsPbBr_3$ perovskite QDs were synthesized modifying a previously reported method (Figure 1).[23] The prepared $CsPbBr_3$ perovskite QDs show a cubic shape and a high morphological uniformity with an average edge length of 10.6 ± 1.2 nm (Figure 1a). High-resolution transmission electron microscopy (HR-TEM) measurement shows orthogonal atomic lattice fringes with a clear visualization of the (200) plane (*d*-spacing of 2.9 Å) and the (110) plane (*d*-spacing of 4.2 Å; Figure 1b), indicating a high crystallinity of the sample. The cubic perovskite crystal phase was confirmed by the powder X-ray diffraction (XRD) measurement with all the Bragg diffraction peak positions matching with the standard (space group: $Pm\bar{3}m$) (Figure 1d). The obtained zwitterionic ligand-capped $CsPbBr_3$ (ZW-$CsPbBr_3$) perovskite QDs exhibit a PL peak centered at 515 nm with a full width at half maximum of 78 meV (ca. 17 nm), similar to that

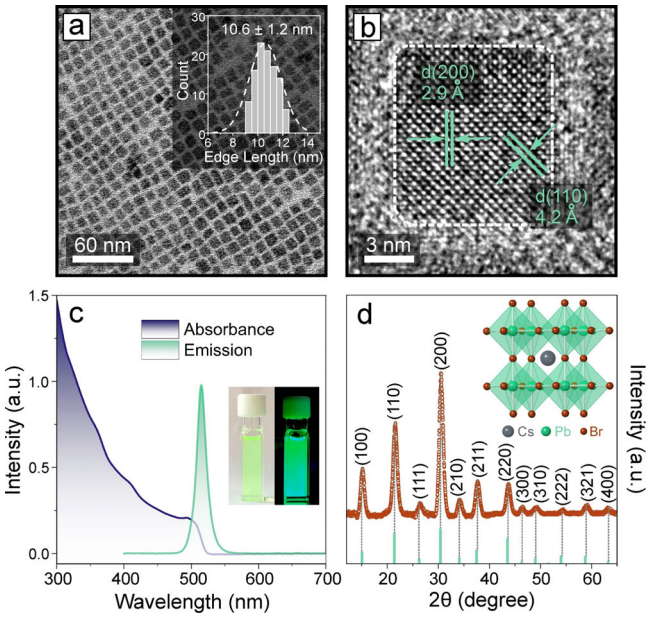

Figure 1. Characterization of ZW-$CsPbBr_3$ perovskite QDs. a) TEM image. Inset: histogram of the edge length distribution. b) HR-TEM image. c) Absorption and emission spectra. Insets: photographs of the QD hexane solution under room light (left) and UV lamp illumination (right). d) XRD pattern of the ZW-$CsPbBr_3$ perovskite QDs. The green bars show the positions of XRD peaks for bulk $CsPbBr_3$.

Table 1: Optimization of reaction conditions.[a]

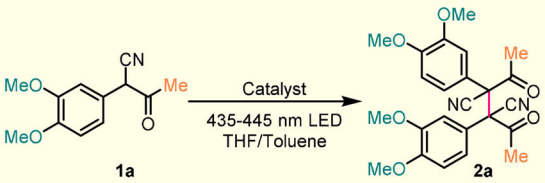

Entry	Catalyst[b]	Ligand of catalyst	Shape	Size distribution [nm][d]	E_{BG} [eV][e]	*t* [h][f]	*dl*/(*dl* + *meso*) [%]	Yield [%][h]
1	CdSe QD	TOP, TOPO, ODPA	sphere	5.2 ± 0.4	2.00	44	> 99	99
2	CdSe QD	OA	sphere	2.9 ± 0.2	2.29	15	> 99	99
3	CdSe-CdS QD	OA, OAm	sphere	6.8 ± 0.5	1.95	63	> 99	94
4	CdS QD	OA	sphere	2.7 ± 0.2	2.82	10	> 99	89
5	CdS-CdSe QD	OA, OAm	sphere	4.6 ± 0.4	2.07	40	> 99	95
6	$CsPbBr_3$ QD	OA, OAm	cube	10.5 ± 0.9	2.39	1	> 99	95
7	$CsPbI_3$ QD	OA, OAm	cube	11.8 ± 0.9	1.80	1	> 99	97
8	$CsPbBr_3$ QD	zwitterion	cube	10.6 ± 1.2	2.40	0.2	> 99	99
9	zwitterion[c]	–	–	–	–	70[g]	ca. 63	20[i]
10	no[j]	–	–	–	–	70[g]	ca. 63	20[i]
11	supernatant[k]	–	–	–	–	0.2	–	0

[a] Reaction conditions: **1a** (0.05 mmol) in THF (0.2 mL) was added to a QD toluene solution (3.2 mL). [b] The optical density (OD) of absorbance was 7.7 at 440 nm for all the catalysts used. For $CsPbBr_3$ QDs, the amount was 1.3×10^{-3} mol%. [c] 0.6 mg (the calculated equivalent amount of ligands used in Entry 8). [d] Diameter for spherical QDs and edge length for cubic QDs. [e] Bandgap energy determined by Tauc plot fitting (Supporting Information, Figure S3). [f] Reaction completion time. [g] Reaction was not complete and stopped after 70 h. [h] High-performance liquid chromatography (HPLC) determined reaction yields (Supporting Information, Figure S4). [i] Light triggered dimerization induced by small spectral overlap between the absorption of **1a** and the LED light (Supporting Information, Figure S5). No reaction occurred under dark. [j] A mixture of *dl* and *meso* isomers (*dl*/*meso* = 15:1; yield, 95%) was detected when photocatalyzed by molecular photocatalyst $[Ru(bpz)_3][PF_6]_2$ (2 mol%) after 50 h (see the Supporting Information). [k] The reaction was run under the conditions in Entry 8 for 5 min, then the QDs were precipitated by addition of methanol. The supernatant was washed using methanol for another three times and the solvent was evaporated to 3.4 mL, then the resulting solution was irradiated for another 0.2 h, in which process no detectable increased amount of product was produced.

of oleate/oleylamine-capped $CsPbBr_3$ (OA/OAm-$CsPbBr_3$) perovskite QDs (Figure 1c).

With different QDs in hand, we started with 2-(3,4-dimethoxyphenyl)-3-oxobutanenitrile (**1a**) as a model substrate to investigate the feasibility of photocatalytic coupling reactions using the QDs as photocatalysts. With two electron-donating methoxy groups on the phenyl ring, **1a** has been reported to convert to benzo[*b*]furan via oxidative intramolecular cyclization[24] or to a dimer via oxidative intermolecular C–C coupling.[21,22] When **1a** was treated with CdSe QDs passivated with surface ligands of trioctylphosphine (TOP), octadecylphosphonic acid (ODPA), trioctylphosphine oxide (TOPO), 99% of the dimer (**2a**) product with negligible amount of benzo[*b*]furan was obtained after 44 h of irradiation using a blue LED light source (435–445 nm) (Table 1, Entry 1). When replacing with OA-CdSe QDs, the reaction time was shortened to 15 h, which can be attributed to the increased permeability of the ligand shell (OA compared to a combination of TOP, TOPO and ODPA) and the increased redox potential due to a smaller size (2.9 nm vs. 5.2 nm, Table 1, Entry 2; Supporting Information, Figure S3). CdSe-CdS core–shell QDs exhibited less photocatalytic reactivity, which can be explained by a strong confinement of photogenerated holes to the CdSe core region, limiting their accessibility to the particle surface for the subsequent oxidative coupling reaction (Table 1, Entry 3).[10a,11a] In contrast, CdS QDs accelerated the reaction to complete in 10 h at the expense of lowering **2a** product yield to 89% (Table 1, Entry 4). We further tested using CdS-CdSe core–shell QDs with a reverse Type-I band gap alignment, in which the photogenerated carriers (both electron and hole) can migrate to the particle surface to participate the reaction.[25] However, neither the reaction rate nor the reaction yield showed any improvements, which was likely ascribed to the narrow band gap (ca. 2.07 eV) induced low oxidation potential of the QDs (Table 1, Entry 5, and Figure S3). Next, OA/OAm-$CsPbX_3$ (X = Br, and I) perovskite QDs were examined and showed a much higher reactivity (reaction completed in 1 h) compared to the conventional Cd-based QDs (Table 1, Entry 6, 7). However, a quick loss of particle integrity during either the course of the photocatalytic reaction (for the case of OA/OAm-$CsPbI_3$ QDs) or the post-reaction purification process (for the case of OA/OAm-$CsPbBr_3$ QDs) constraints their photocatalytic performance in a non-recyclable fashion (Supporting Information, Figure S6). To overcome the particle stability issue, zwitterionic capping ligands that can tightly coordinate to both the surface cations and anions of the perovskite QDs were used to replace OA/OAm ligands.[23] In particular, ZW-$CsPbBr_3$ QDs capped with DMOA-PS were tested in the photocatalytic reaction. Remarkably, not only can the ZW-$CsPbBr_3$ QDs be recycled for at least three rounds of reaction-purification cycles (Supporting Information, Figures S7–S9), but the reaction time was also reduced to merely 0.2 h with a high product yield of 99% (Table 1, Entry 8). This enhanced reactivity can be explained by a reduced density of surface ligand coverage (3.0/nm^2 for ZW-$CsPbBr_3$ QDs comparing to 5.4/nm^2 for OA/OAm-$CsPbBr_3$ QDs; Supporting Information, Figures S10–S12 and detailed calculations therein), and thus an increased permeability of the substrates to the particle surface, leading to an increased amount of the substrate adsorbed on the QD surface and lowering the kinetic barrier of the reaction.[8a,b,12] Control experiments with either no catalyst addition or addition of only zwitterionic ligands (that is, DMOA-PS) without QDs or supernatant solution after precipitation of QDs showed no catalytic effect (Table 1, Entry 9–11), confirming the catalytic role of the ZW-$CsPbBr_3$ perovskite QDs.

To unravel the catalytic role of the $CsPbBr_3$ perovskite QDs play in the C–C coupling reaction, a kinetic study was carried out and the reaction order was examined by monitoring the concentration evolution of product **2a** using high performance liquid chromatography (HPLC). The concentration of **2a** increased linearly as a function of the reaction time with a rate constant (k) of $1.17\times10^{-5}\,M\,s^{-1}$ ($3.33\times10^{-6}\,M\,s^{-1}$ for OA/OAm-$CsPbBr_3$ QDs), and then remained nearly constant ($7.4\times10^{-3}\,M$) upon consumption of **1a** substrates (Figure 2; Supporting Information, Figures S4, S13). This result suggests a zero-order reaction with respect to the reactant, **1a**, signifying the catalytic nature of the coupling reaction. Importantly, in contrast to resulting in a mixture of *dl*- and *meso*-isomers (*dl*/*meso* = 5:3, Table 1) for the reactions without QD catalysts, all the QDs photocatalyzed reactions studied here showed a stereoselectivity of *dl*-isomer over *meso*-isomer (> 99%, Table 1; Supporting Information). Such a high stereoselectivity cannot be obtained with any conventional oxidants[21b] or catalytic metal complex.[21a]

To further expand the scope of the photocatalytic reaction, various α-aryl ketonitriles with different R^1 and R^2 groups as substrates were examined under the optimized reaction conditions using ZW-$CsPbBr_3$ perovskite QDs as catalysts, and the results are summarized in Figure 3. Since the dimerization reactions studied in our system are likely through a radical mediated reaction pathway, different EDGs and conjugated π systems, both of which can stabilize free radical intermediates,[26] were chosen as R^1 substituents on the benzene ring of substrates. In particular, the substrates bearing EDGs (that is, 3,4-dimethoxy, 3,4-methylenedioxy, and 4-methoxy) at the *para*-position of the benzene ring could produce the corresponding dimers efficiently (reaction yield > 90% within 30 mins, Figure 3, **2a–c**; Supporting Information, Figures S14, S15). Whereas, no desired products were produced when the EDGs (that is, methoxy group) were

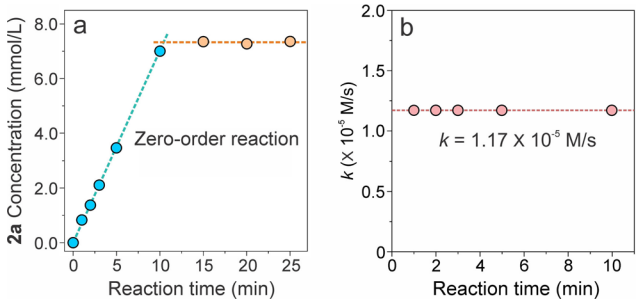

Figure 2. Concentration evolution of product **2a** (a) and reaction rate constant (b) as a function of reaction time under optimized reaction conditions.

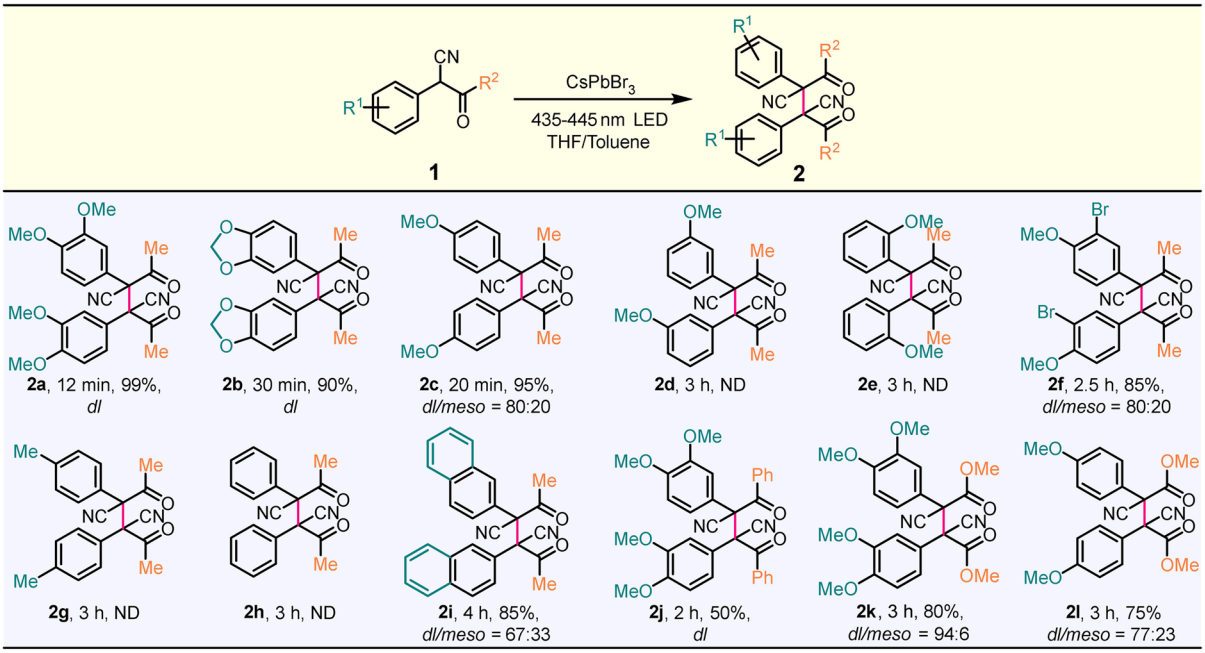

Figure 3. Oxidative dimerization of α-aryl ketonitriles photocatalyzed by ZW-$CsPbBr_3$ perovskite QDs. General conditions: substrate **1** (0.05 mmol) in a THF (0.2 mL) was added to a solution of $CsPbBr_3$ QDs in toluene (3.2 mL, OD at 440 nm = 7.7) in a 4 mL vial, and the resulting mixture was irradiated using a blue LED (435–445 nm) light source at room temperature. The labeled reaction time indicates the reaction completion time. The yields are isolated yields after silica gel chromatography. ND: no desired product.

placed at the *ortho*- or *meta*-positions (Figure 3, **2d**, **e**). The less electron-donating effect from the methoxy group at *meta*-position leads to an increased oxidation potential required for the dimerization, resulting in the product yield staying at a negligible level (Figure 3, **2d**). Although the methoxy group at the *ortho*-position provides a stronger electron-donating effect, the steric hindrance induced by close proximity between the *ortho*-methoxy group and the benzylic position (reaction site) reasonably explains the failure of the dimerization reaction (Figure 3, **2e**). While retaining the *para*-methoxy group, and adding a *meta*-bromo group as an electron-withdrawing substituent, the reduced effect in electron donating of the substrate cause a slower dimerization reaction (reaction completion time of 2.5 h) with a lowered reaction yield of 85% mixed dimers (*dl*/*meso* = 80:20; Figure 3, **2f**). To further demonstrate the requisite of strong electron donating effect in the dimerization reaction, the substrates either with a weaker EDG (that is, methyl group) on the *para*-position or without any functional groups on the aromatic ring were tested and brought no desired dimer products as expected (Figure 3, **2g**, **h**). Alternative to the addition of EDGs, expansion of the conjugated π-system of the substrate can also stabilize free radical intermediates through electron delocalization effect.[26] Evidently, replacing the benzene ring with a naphthyl group on the substrate delivered desired dimer products (*dl*/*meso* = 67:33) with a yield of 85% in a 4-h reaction time (Figure 3, **2i**). Besides varying R^1 substituents, we further expand the reaction scope by altering the R^2 substituent from methyl group to aryl (Figure 3, **2j**) or methoxy group (Figure 3, **2k**, **l**). In all cases, the dimerization reaction occurred to generate the corresponding products with reasonable reaction yields (≥50%, Figure 3, **2j–l**). The *dl*- and *meso*-isomers were distinguished using nuclear magnetic resonance (NMR) spectroscopy, in which *meso*-isomers exhibit a broad single peak at a chemical shift of around 2.35 ppm (a sharp peak for *dl*-isomer at around 2.45 ppm) for COMe group (see NMR spectra in the Supporting Information).[21] The assignments were confirmed by variable temperature NMR and heteronuclear single quantum coherence spectroscopy (HSQC) measurements using **2c** as an example (see discussion in the Supporting Information, Figures S14, S15).

It is known that α-aryl ketonitriles can be converted to either dimers or benzo[*b*]furans under oxidative conditions.[21a,24] Specifically, intermediate radicals of **1a-1** or **1a-2** need to be generated through dissociating either $C–H^1$ or $C–H^2$ bond, respectively for the subsequent formation of dimer (from **1a-1**) or benzo[*b*]furan (from **1a-2**). However, in our reaction system, only dimer products were collected for all the substrates inspected (Figure 3). To understand the underlining mechanism, the bond dissociation energies for $C–H^1$ and $C–H^2$ bonds were calculated using density functional theory (DFT) calculations (see the Supporting Information). A 62% smaller bond dissociation energy of 71 kcal mol^{-1} was obtained for the $C–H^1$ bond than that of the $C-H^2$ bond (dissociation energy of 115 kcal mol^{-1}), indicating **1a-1** radical is the energetically favored product (Figure 4a). The DFT calculation result is in good agreement with the sole observation of dimer products (Table 1). To further confirm the presence of the tertiary carbon radical (**1a-1**) formed from $C–H^1$ bond cleavage, electron paramagnetic resonance (EPR) spectroscopy measurements were carried out using 5,5-dimethyl-pyrroline *N*-oxide (DMPO) as a radical scavenger.[15b] Under the optimized reaction conditions, however

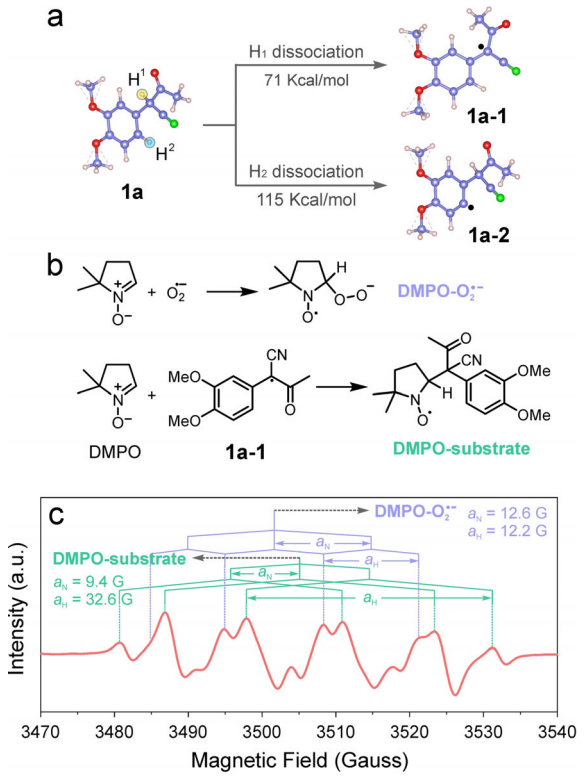

Figure 4. Mechanism study of photo-induced oxidative coupling of 2-(3,4-dimethoxyphenyl)-3-oxobutanenitrile (**1a**). a) Bond dissociation energies of the C–H^1 and C–H^2 bonds of 2-(3,4-dimethoxyphenyl)-3-oxobutanenitrile (**1a**) calculated by DFT. b) Reaction schemes showing the generation of DMPO-superoxide and DMPO-substrate species upon addition of radical trapping agent DMPO. c) EPR spectrum of a toluene/THF solution mixture of $CsPbBr_3$ QDs, DMPO and 2-(3,4-dimethoxyphenyl)-3-oxobutanenitrile (**1a**,) after irradiation for 20 min.

with absence of substrate **1a** (see the Supporting Information for details), a four-fold EPR signal with a hyperfine coupling constant of N atom (a_N) of 12.8 G and a coupling constant of H atom (a_H) of 8.3 G (g value: 2.010) was detected and assigned to DMPO-superoxide adduct after 5-second illumination using a LED light source (435–445 nm) (Supporting Information, Figure S16).[15a] A three-fold hyperfine splitting profile (a_N: 13.1 G and g value: 2.009) was observed with further illumination for a total of 20 min, as a result of the ring-opening of the DMPO-superoxide adduct (Supporting Information, Figure S16).[15b] When substrate **1a** was introduced to the reaction solution, an EPR signal with two sets of hyperfine splitting patterns were obtained (Figure 4c). Detailed EPR signal analysis showed the presence of two active species, that is, DMPO-superoxide (a_N: 12.6 G, a_H: 12.2 G; and g value: 2.012) and DMPO-substrate-**1a-1** species (a_N: 9.4 G; a_H: 32.6 G; and g value: 2.010) (Figure 4b,c).[6b] For each of the species, EPR signal first split into a triplet from the interaction between the radical (**1a-1**) and N nucleus, and then further split into quartet (for DMPO-superoxide species) and sextet (for DMPO-substrate-**1a-1** species) as results of the interaction with H nucleus (Figure 4c). The EPR results unambiguously proved the formation of substrate **1a-1** radicals in the reaction. Together, both the bond dissociation energy calculation and EPR results agree well with the experimentally observed exclusive dimerization reaction, strongly supporting the proposed free-radical-based reaction pathway.

Our photocatalytic reaction results and mechanistic studies clearly delineated a proposed reaction mechanism as shown in Figure 5. During the reaction, after absorbing an excitation photon, one electron will be excited to the conduction band (CB) of the $CsPbBr_3$ perovskite QD and then consumed by reacting with a surrounded O_2 molecule to form superoxide radical ($O_2^{\bullet-}$). Meanwhile, the hole left in the valence band (VB) oxidizes the substrate molecule (such as **1a**) to form radical intermediates (**1a-1**; Figure 5). Given the Pb-rich surface nature of the $CsPbBr_3$ perovskite QDs (Supporting Information, Figure S17), the reactants and resultant free radical intermediates can dynamically attach to surface Pb^{2+} ions through donating a lone pair of electrons of the oxygen atom in the carbonyl group, acting as a L-type ligand, which was supported by the broadening and shifting of the *CH* and $COCH_3$ peaks of the substrate in the NMR spectra (Supporting Information, Figure S18).[18,27] Consequently, dimer products can be formed by the C–C bond formation between two neighboring radicals. Depending on the relative configuration of the two radicals on the QD surfaces, either *dl*- or *meso*-isomers can be obtained (Figure 5). However, less steric hinderance between the aryl groups of the radicals in the *trans*-arrangement makes the *dl*-isomer a kinetically favored reaction product (Figure 5). The same *dl*-configuration is also a thermodynamically favored geometry because of the attractive interaction between the *gauche* cyano groups upon molecular structural relaxation after detaching from the QD surfaces.[28] Furthermore, the reactions using the substrates with relatively large substituent groups delivered pure *dl*-isomers (Figure 3, **2a**, **b**, **j**), strongly supporting our hypothesis of steric hinderance induced stereoselectivity. To confirm that the photogenerated hole, rather than the in situ formed superoxide species ($O_2^{\bullet-}$), is

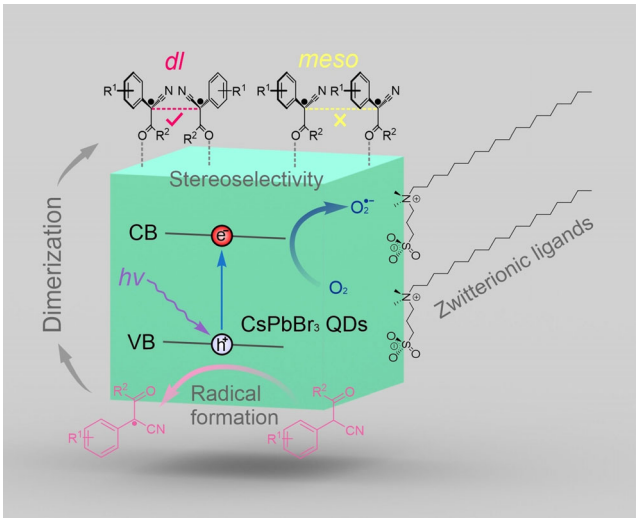

Figure 5. Proposed reaction scheme for the stereoselective dimerization of α-aryl ketonitriles photocatalyzed by ZW-$CsPbBr_3$ perovskite QDs.

acting as the oxidative reagent for the dimerization reaction, substrate **1a** was directly treated with superoxide (see the Supporting Information). The result of undetectable dimer products further supports the proposed monomer radical mediated reaction mechanism (Figure 5).

Conclusion

We show the first example of stereoselective C–C oxidative dimerization reaction photocatalyzed by ZW-$CsPbBr_3$ perovskite QDs under visible light illumination. High stereoselectivities (>99%) of *dl*-isomer are demonstrated by dimerizing two α-aryl ketonitriles. We found that the zwitterionic ligand coverage is crucial to stabilize/recycle the QD catalysts as well as enhance their photocatalytic reactivity. Moreover, we expand the reaction scope by investigating a series of starting substrate materials with different substituents on the aryl ring and varied functional moieties. We show that EDGs on the *para*-position of the aryl ring or an extended conjugated π system is necessity for efficient dimerization reactions to occur. Furthermore, mechanistic studies reveal a free-radical mediated reaction pathway with the steric hinderance effect being largely responsible for the observed stereoselectivity. Our study shows that lead halide perovskite QDs with an optimized ligand passivation hold a great potential of acting as efficient photocatalysts in a range of organic transformations with improved product yield and high selectivity.

Acknowledgements

O.C. acknowledges the supports from Brown University startup funds and the National Science Foundation (CBET-1936223 and DMR-1943930). TEM measurements were performed at the Electron Microscopy Facility in IMNI at Brown University.

Conflict of interest

The authors declare no conflict of interest.

Keywords: C–C coupling · $CsPbBr_3$ · perovskite QDs · photocatalysis · stereoselectivity

[1] a) G. H. Carey, A. L. Abdelhady, Z. Ning, S. M. Thon, O. M. Bakr, E. H. Sargent, *Chem. Rev.* **2015**, *115*, 12732 – 12763; b) H. Yang, Y. Zhang, K. Hills-Kimball, Y. Zhou, O. Chen, *Sustainable Energy Fuels* **2018**, *2*, 2381 – 2397; c) J. Wang, Y. Yuan, H. Zhu, T. Cai, Y. Fang, O. Chen, *Nano Energy* **2020**, *67*, 104217.

[2] a) I. L. Medintz, H. T. Uyeda, E. R. Goldman, H. Mattoussi, *Nat. Mater.* **2005**, *4*, 435 – 446; b) J. K. Jaiswal, S. M. Simon, *Trends Cell Biol.* **2004**, *14*, 497 – 504; c) M.-K. So, C. Xu, A. M. Loening, S. S. Gambhir, J. Rao, *Nat. Biotechnol.* **2006**, *24*, 339 – 343; d) M. Heine, A. W. Fischer, C. Schlein, C. Jung, L. G. Straub, K. Gottschling, N. Mangels, Y. Yuan, S. K. Nilsson, G. Liebscher, O. Chen, R. Schreiber, R. Zechner, L. Scheja, J. Heeren, *Cell Metab.* **2018**, *28*, 644 – 655; e) O. T. Bruns, T. S. Bischof, D. K. Harris, D. Franke, Y. Shi, L. Riedemann, A. Bartelt, F. B. Jaworski, J. A. Carr, C. J. Rowlands, M. W. B. Wilson, O. Chen, H. Wei, G. W. Hwang, D. M. Montana, I. Coropceanu, O. B. Achorn, J. Kloepper, J. Heeren, P. T. C. So, D. Fukumura, K. F. Jensen, R. K. Jain, M. G. Bawendi, *Nat. Biomed. Eng.* **2017**, *1*, 0056.

[3] a) Q. Sun, Y. A. Wang, L. S. Li, D. Wang, T. Zhu, J. Xu, C. Yang, Y. Li, *Nat. Photonics* **2007**, *1*, 717 – 722; b) X. Dai, Z. Zhang, Y. Jin, Y. Niu, H. Cao, X. Liang, L. Chen, J. Wang, X. Peng, *Nature* **2014**, *515*, 96 – 99; c) L. Qian, Y. Zheng, J. Xue, P. H. Holloway, *Nat. Photonics* **2011**, *5*, 543 – 548; d) Y.-H. Won, O. Cho, T. Kim, D.-Y. Chung, T. Kim, H. Chung, H. Jang, J. Lee, D. Kim, E. Jang, *Nature* **2019**, *575*, 634 – 638.

[4] a) M. Lu, Y. Zhang, S. X. Wang, J. Guo, W. W. Yu, A. L. Rogach, *Adv. Funct. Mater.* **2019**, *29*, 1902008; b) E. Jang, Y. Kim, Y. H. Won, H. Jang, S. M. Choi, *ACS Energy Lett.* **2020**, *5*, 1316 – 1327; c) J. H. Jo, D. Y. Jo, S. H. Lee, S. Y. Yoon, H. B. Lim, B. J. Lee, Y. R. Do, H. Yang, *ACS Appl. Nano Mater.* **2020**, *3*, 1972 – 1980.

[5] a) L. Gao, L. N. Quan, F. P. García de Arquer, Y. Zhao, R. Munir, A. Proppe, R. Quintero-Bermudez, C. Zou, Z. Yang, M. I. Saidaminov, O. Voznyy, S. Kinge, Z. Lu, S. O. Kelley, A. Amassian, J. Tang, E. H. Sargent, *Nat. Photonics* **2020**, *14*, 227 – 233; b) Y. Yuan, H. Zhu, X. Wang, D. Cui, Z. Gao, D. Su, J. Zhao, O. Chen, *Chem. Mater.* **2019**, *31*, 2635 – 2643; c) O. Chen, H. Wei, A. Maurice, M. Bawendi, P. Reiss, *MRS Bull.* **2013**, *38*, 696 – 702; d) M. V. Kovalenko, L. Manna, A. Cabot, Z. Hens, D. V. Talapin, C. R. Kagan, V. I. Klimov, A. L. Rogach, P. Reiss, D. J. Milliron, P. Guyot-Sionnnest, G. Konstantatos, W. J. Parak, T. Hyeon, B. A. Korgel, C. B. Murray, W. Heiss, *ACS Nano* **2015**, *9*, 1012 – 1057; e) T. Cai, W. Shi, S. Hwang, K. Kobbekaduwa, Y. Nagaoka, H. Yang, K. Hills-Kimball, H. Zhu, J. Wang, Z. Wang, Y. Liu, D. Su, J. Gao, O. Chen, *J. Am. Chem. Soc.* **2020**, *142*, 11927 – 11936.

[6] a) K. Chen, X. Deng, G. Dodekatos, H. Tüysüz, *J. Am. Chem. Soc.* **2017**, *139*, 12267 – 12273; b) Q. Guo, F. Liang, X.-B. Li, Y.-J. Gao, M.-Y. Huang, Y. Wang, S.-G. Xia, X.-Y. Gao, Q.-C. Gan, Z.-S. Lin, C.-H. Tung, L.-Z. Wu, *Chem* **2019**, *5*, 2605 – 2616; c) K. P. McClelland, E. A. Weiss, *ACS Appl. Energy Mater.* **2019**, *2*, 92 – 96.

[7] a) W. Wu, G. Liu, Q. Xie, S. Liang, H. Zheng, R. Yuan, W. Su, L. Wu, *Green Chem.* **2012**, *14*, 1705 – 1709; b) S. C. Jensen, S. Bettis Homan, E. A. Weiss, *J. Am. Chem. Soc.* **2016**, *138*, 1591 – 1600; c) X. Zhu, Y. Lin, Y. Sun, M. C. Beard, Y. Yan, *J. Am. Chem. Soc.* **2019**, *141*, 733 – 738.

[8] a) J. A. Caputo, L. C. Frenette, N. Zhao, K. L. Sowers, T. D. Krauss, D. J. Weix, *J. Am. Chem. Soc.* **2017**, *139*, 4250 – 4253; b) Z. Zhang, K. Edme, S. Lian, E. A. Weiss, *J. Am. Chem. Soc.* **2017**, *139*, 4246 – 4249; c) Z. Hong, W. K. Chong, A. Y. R. Ng, M. Li, R. Ganguly, T. C. Sum, H. S. Soo, *Angew. Chem. Int. Ed.* **2019**, *58*, 3456 – 3460; *Angew. Chem.* **2019**, *131*, 3494 – 3498; d) Y. Jiang, C. Wang, C. R. Rogers, M. S. Kodaimati, E. A Weiss, *Nat. Chem.* **2019**, *11*, 1034 – 1040; e) X. Zhu, Y. Lin, J. San Martin, Y. Sun, D. Zhu, Y. Yan, *Nat. Commun.* **2019**, *10*, 2843.

[9] W. W. Yu, L. Qu, W. Guo, X. Peng, *Chem. Mater.* **2003**, *15*, 2854 – 2860.

[10] a) O. Chen, J. Zhao, V. P. Chauhan, J. Cui, C. Wong, D. K. Harris, H. Wei, H.-S. Han, D. Fukumura, R. K. Jain, M. G. Bawendi, *Nat. Mater.* **2013**, *12*, 445 – 451; b) Q. Zhong, M. Cao, Y. Xu, P. Li, Y. Zhang, H. Hu, D. Yang, Y. Xu, L. Wang, Y. Li, X. Zhang, Q. Zhang, *Nano Lett.* **2019**, *19*, 4151 – 4157.

[11] a) R. Tan, Y. Yuan, Y. Nagaoka, D. Eggert, X. Wang, S. Thota, P. Guo, H. Yang, J. Zhao, O. Chen, *Chem. Mater.* **2017**, *29*, 4097 – 4108; b) L. Protesescu, S. Yakunin, M. I. Bodnarchuk, F. Krieg, R. Caputo, C. H. Hendon, R. X. Yang, A. Walsh, M. V. Kovalenko, *Nano Lett.* **2015**, *15*, 3692 – 3696.

[12] M. S. Kodaimati, K. P. McClelland, C. He, S. Lian, Y. Jiang, Z. Zhang, E. A. Weiss, *Inorg. Chem.* **2018**, *57*, 3659 – 3670.

[13] a) C. Huang, X.-B. Li, C.-H. Tung, L.-Z. Wu, *Chem. Eur. J.* **2018**, *24*, 11530 – 11534; b) I. N. Chakraborty, S. Roy, G. Devatha, A. Rao, P. P. Pillai, *Chem. Mater.* **2019**, *31*, 2258 – 2262.
[14] A. Pal, I. Ghosh, S. Sapra, B. König, *Chem. Mater.* **2017**, *29*, 5225 – 5231.
[15] a) H. Huang, H. Yuan, K. P. F. Janssen, G. Solís-Fernández, Y. Wang, C. Y. X. Tan, D. Jonckheere, E. Debroye, J. Long, J. Hendrix, J. Hofkens, J. A. Steele, M. B. J. Roeffaers, *ACS Energy Lett.* **2018**, *3*, 755 – 759; b) S. Schünemann, M. van Gastel, H. Tüysüz, *ChemSusChem* **2018**, *11*, 2057 – 2061; c) S. Xie, Z. Shen, J. Deng, P. Guo, Q. Zhang, H. Zhang, C. Ma, Z. Jiang, J. Cheng, D. Deng, Y. Wang, *Nat. Commun.* **2018**, *9*, 1181.
[16] Y. Huang, Y. Zhu, E. Egap, *ACS Macro Lett.* **2018**, *7*, 184 – 189.
[17] J. Hu, T.-J. Pu, Z.-W. Xu, W.-Y. Xu, Y.-S. Feng, *Adv. Synth. Catal.* **2019**, *361*, 708 – 713.
[18] J. De Roo, M. Ibáñez, P. Geiregat, G. Nedelcu, W. Walravens, J. Maes, J. C. Martins, I. Van Driessche, M. V. Kovalenko, Z. Hens, *ACS Nano* **2016**, *10*, 2071 – 2081.
[19] Z. Zhang, Y. Liang, H. Huang, X. Liu, Q. Li, L. Chen, D. Xu, *Angew. Chem. Int. Ed.* **2019**, *58*, 7263 – 7267; *Angew. Chem.* **2019**, *131*, 7341 – 7345.
[20] W.-B. Wu, Y.-C. Wong, Z.-K. Tan, J. Wu, *Catal. Sci. Technol.* **2018**, *8*, 4257 – 4263.
[21] a) H. A. P. De Jongh, C. R. H. I. De Jonge, W. J. Mijs, *J. Org. Chem.* **1971**, *36*, 3160 – 3168; b) Y. Du, Y. Zhang, S. Wang, K. Zhao, *Synlett* **2009**, 1835 – 1841.
[22] L. Liu, Y. Fan, Q. He, Y. Zhang, D. Zhang-Negrerie, J. Huang, Y. Du, K. Zhao, *J. Org. Chem.* **2012**, *77*, 3997 – 4004.
[23] F. Krieg, S. T. Ochsenbein, S. Yakunin, S. ten Brinck, P. Aellen, A. Süess, B. Clerc, D. Guggisberg, O. Nazarenko, Y. Shynkarenko, S. Kumar, C.-J. Shih, I. Infante, M. V. Kovalenko, *ACS Energy Lett.* **2018**, *3*, 641 – 646.
[24] Z. Liang, W. Hou, Y. Du, Y. Zhang, Y. Pan, D. Mao, K. Zhao, *Org. Lett.* **2009**, *11*, 4978 – 4981.
[25] a) Z. Pan, H. Zhang, K. Cheng, Y. Hou, J. Hua, X. Zhong, *ACS Nano* **2012**, *6*, 3982 – 3991; b) P. Wang, M. Wang, J. Zhang, C. Li, X. Xu, Y. Jin, *ACS Appl. Mater. Interfaces* **2017**, *9*, 35712 – 35720.
[26] D. Griller, K. U. Ingold, *Acc. Chem. Res.* **1976**, *9*, 13 – 19.
[27] K. Hills-Kimball, M. J. Pérez, Y. Nagaoka, T. Cai, H. Yang, A. H. Davis, W. Zheng, O. Chen, *Chem. Mater.* **2020**, *32*, 2489 – 2500.
[28] L. I. Peterson, *J. Am. Chem. Soc.* **1967**, *89*, 2677 – 2681.

Manuscript received: May 25, 2020
Revised manuscript received: August 12, 2020
Accepted manuscript online: August 27, 2020
Version of record online: ■■ ■■, ■■■■

Research Articles

Perovskites

Y. Yuan, H. Zhu, K. Hills-Kimball, T. Cai, W. Shi, Z. Wei, H. Yang, Y. Candler, P. Wang, J. He, O. Chen* ____ ▮▮▮▮–▮▮▮▮

Stereoselective C—C Oxidative Coupling Reactions Photocatalyzed by Zwitterionic Ligand Capped $CsPbBr_3$ Perovskite Quantum Dots

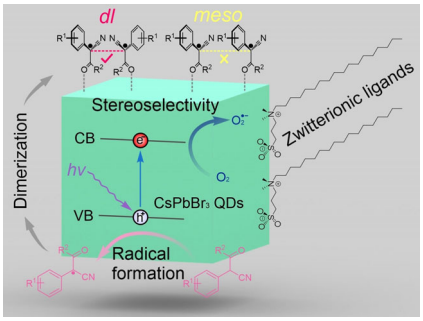

C—C oxidative dimerizations of α-aryl ketonitriles are realized by using zwitterionic ligand capped $CsPbBr_3$ perovskite QDs as catalysts under visible light illumination, via a radical mediated reaction pathway. High stereoselectivities of *dl*-isomers were obtained owing to less steric hindrance during the bond formation process. Our study sheds new lights on using lead-halide perovskite QDs as photocatalysts for stereoselective organic synthesis.